PERGAMON

Deep-Sea Research II 49 (2002) 1073–1079

DEEP-SEA RESEARCH
PART II

www.elsevier.com/locate/dsr2

Impact tsunami–Eltanin

Steven N. Ward[a,*], Erik Asphaug[b]

[a] *Institute of Geophysics and Planetary Physics, University of California, Santa Cruz, CA 95064, USA*
[b] *Earth Science Board, University of California, Santa Cruz, CA 95064, USA*

Abstract

Employing classical tsunami theory and elementary assumptions about the initial shape of impact cavities, we compute tsunami from the Eltanin asteroid collision at 2.15 Ma. An Eltanin impactor 4 km in diameter would have blown an initial cavity as deep as the ocean and 60 km wide into the South Pacific and delivered a 200–300 m high tsunami to the Antarctic Peninsula and the southern tip of South America 1200–1500 km away. New Zealand, 6000 km distant, would have met 60 m waves. Generalizing these results to other size impactors, we fit simplified tsunami attenuation laws to maximum tsunami heights extracted from the full-wave calculations. If Eltanin was 1 km in diameter instead of 4 km, its waves would have been at least five times smaller. An asteroid the size of Chicxulub (10 km diameter), had it fallen into water deeper than 1000 m, would have sent a 100 m tsunami out to 4000 km distance, even if shoaling amplifications are neglected.

1. Impact tsunami theory

Imagine that the initial stage of cratering by an asteroid impact at position $\mathbf{r}_0$ excavates a radially symmetric, parabolic cavity of depth D_c and inner and outer radii R_C and R_D described by

$$u_z^{\text{impact}}(\mathbf{r}) = D_c(1 - |\mathbf{r} - \mathbf{r}_0|^2/R_C^2) \quad |\mathbf{r} - \mathbf{r}_0| \leqslant R_D;$$

$$u_z^{\text{impact}}(\mathbf{r}) = 0 \quad |\mathbf{r} - \mathbf{r}_0| > R_D. \tag{1}$$

We consider the case $R_D = \sqrt{2}R_C$, where all of the excavated material deposits on the crater lip between radius R_C and R_D. Under classical, linear tsunami theory (Ben-Menahem and Singh, 1981; Dingemans, 1997; Ward and Asphaug, 2000; Ward, 2001a, b) transient initial cavity (1) evolves to propagating tsunami waves at observation point $\mathbf{r}$ and time t as

$$u_z^{\text{surf}}(\mathbf{r}, \mathbf{r}_0, t) = \int_0^\infty \frac{k(\omega, h(\mathbf{r}_0))\cos(\omega t)\,\mathrm{d}\omega}{2\pi u(\omega, h(\mathbf{r}_0))} \times F(k(\omega, h(\mathbf{r}_0)), R_C, R_D) \times J_0(\omega T(\omega, \mathbf{r}, \mathbf{r}_0))\, G(\mathbf{r}, \mathbf{r}_0) S_L(\omega, \mathbf{r}, \mathbf{r}_0). \tag{2}$$

In (2) and below $k(\omega, h)$ is the wavenumber associated with a tsunami of frequency ω in an ocean of depth h. Wavenumber satisfies the dispersion relation

$$\omega^2 = gk(\omega, h)\tanh[k(\omega, h)h], \tag{3}$$

where g is the acceleration of gravity. In classical theory the phase $c(\omega, h)$ and group velocity $u(\omega, h)$

*Corresponding author. Fax: +1-831-459-3074.
E-mail address: ward@uplift.ucsc.edu (S.N. Ward).

0967-0645/02/$ - see front matter
PII: S0967-0645(01)00147-3

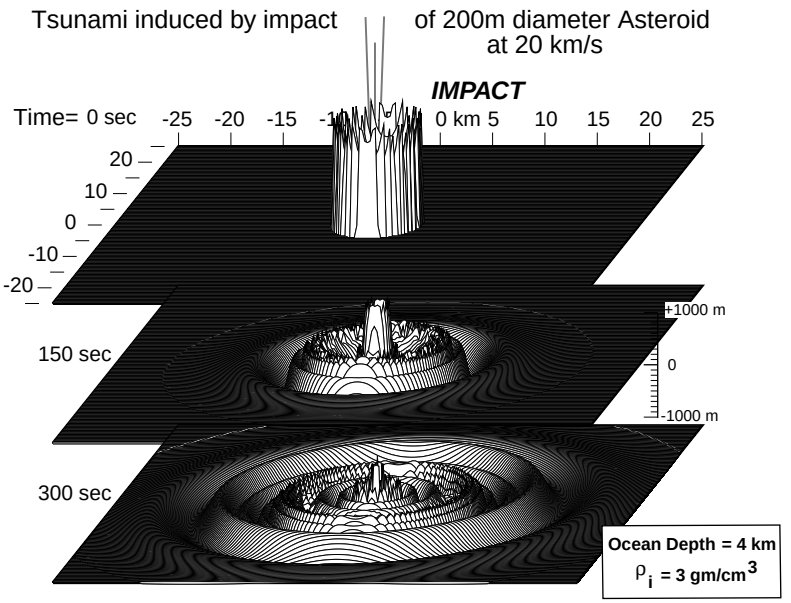

Fig. 1. Impact tsunami calculated from Eq. (2) in a uniform depth ocean (4000 m). Note that impact tsunami involve a great sequence of waves—low frequency, long waves travel fastest, shorter waves trail. The leading wave in the bottom panel is about 325 m high.

of gravity waves are

$$c(\omega,h)=\sqrt{\frac{gh\tanh[k(\omega,h)h]}{k(\omega,h)h}}$$

and

$$u(\omega,h)=c(\omega,h)\left[\frac{1}{2}+\frac{k(\omega,h)h}{\sinh[2k(\omega,h)h]}\right].$$

Other elements in (2) include:

- A travel time $T(\omega,\mathbf{r},\mathbf{r}_0)$ of tsunami of frequency ω: $T(\omega,\mathbf{r},\mathbf{r}_0)=\int_{\text{ray path}} \mathrm{d}p/c(\omega,h(\mathbf{p}))$.
- A geometrical spreading correction factor $G(r,r_0)$ that for tsunami on a sphere is expressed adequately by

$$G(\mathbf{r},\mathbf{r}_0)=G(\Delta)=\sqrt{\frac{\Delta}{\sin\Delta}}. \quad (4)$$

  Δ measures angular distance from $\mathbf{r}_0$ to $\mathbf{r}$.
- A shoaling factor $S_{\mathrm{L}}(\omega,r,r_0)$ that under linear theory is

$$S_{\mathrm{L}}(\omega,\mathbf{r},\mathbf{r}_0)=\sqrt{\frac{u(\omega,h(\mathbf{r}_0))}{u(\omega,h(\mathbf{r}))}}. \quad (5)$$

- A wavenumber spectrum of transient cavity (1)

$$F(k,R_{\mathrm{C}},R_{\mathrm{D}})=\frac{4\pi R_{\mathrm{D}}^2 D_{\mathrm{c}}}{k^2R_{\mathrm{C}}^2}\times[J_2(kR_{\mathrm{D}})-k(R_{\mathrm{D}}^2-R_{\mathrm{C}}^2)\times J_1(kR_{\mathrm{D}})/2R_{\mathrm{D}}]. \quad (6)$$

  The $J_n(x)$ in (2) and (6) are cylindrical Bessel functions.

Fig. 1 evaluates (2) at times 0, 150 and 300 s over a 50 km^2 section of ocean adjacent to a transient impact cavity 2126 m deep and 5.8 km across. This size of cavity would be dug by a 20 km/s water impact of a 200 m diameter stony asteroid (see below).

2. Crater shape relations

To use formula (2) for asteroid impacts cavity depth D_{c} and cavity radius R_{C} have to be established from impactor properties. For cavity diameter $d_{\mathrm{c}}=2R_{\mathrm{C}}$ we employ the familiar scaling rule of Schmidt and Holsapple

(1982)

$$d_c^{S-H} = 2R_I\left[\left(\frac{1}{3.22}\right)\frac{V_I^2}{gR_I}\right]^{\beta}\left(\frac{\rho_I}{\rho_T}\right)^{1/3}\left\{\frac{C_T}{1.24}\right\}. \quad (7)$$

In (7) R_I V_I and ρ_I label the radius, velocity and density of the impactor. Parameters $\beta = 0.22$ and $C_T = 1.88$ depend on target properties and derive from laboratory impact experiments into water. If cavities of shape (1) have a general relationship between depth and radius as

$$D_c = qR_C^{\alpha} \quad (8)$$

Ward and Asphaug (2000) showed by means of basic energy arguments that crater diameter relates to impactor properties as

$$d_c = 2R_I\left[(2\varepsilon)\frac{V_I^2}{gR_I}\right]^{\delta} \times \left(\frac{\rho_I}{\rho_T}\right)^{1/3}\left\{\left(\frac{\rho_T}{\rho_I}\right)^{1/3-\delta}\left(\frac{1}{qR_I^{\alpha-1}}\right)^{2\delta}\right\}. \quad (9)$$

In (9), $\delta = 1/2(1+\alpha)$ and ε is the fraction of impactor kinetic energy that transfers to the tsunami. Formulas (7) and (9) are very similar; in fact, with $\alpha = 1/(2\beta) - 1$ and $\varepsilon = 0.15$, (9) can be solved for q such that they agree identically. With α and q known, (8) associates a cavity depth with a Schmidt–Holsapple crater diameter.

Fig. 2 plots $d_c(R_I)$ and $D_c(R_I)$ determined from Eqs. (7)–(9) for $V_I = 20$ km/s, $\rho_I = 3$ gm/cm^3 and $\rho_T = 1$ gm/cm^3. In our range of interest, cavity diameter and depth can be approximated by

$$d_c(R_I) = QR_I^{3/4}; \quad Q = 196.545\, m^{1/4} \quad (10)$$

and

$$D_c(R_I) = d_c(R_I)/3.132. \quad (11)$$

For stony asteroids of radius $R_I = 100$, 1000, and 5000 m, (7–9) return crater depths and diameters of 2.1, 11.2, 35.6 km and 5.8, 34.9, 122.6 km, respectively. The values for $R_I = 100$ m were used in Fig. 1.

Bolides of diameter greater than 300 m will likely cavitate the entire ocean and begin to excavate the seabed. For the purpose of computing tsunami from impacts, Ward and Asphaug (2000) argued that the cavity depth placed into (1) should not exceed the depth of the ocean at the impact

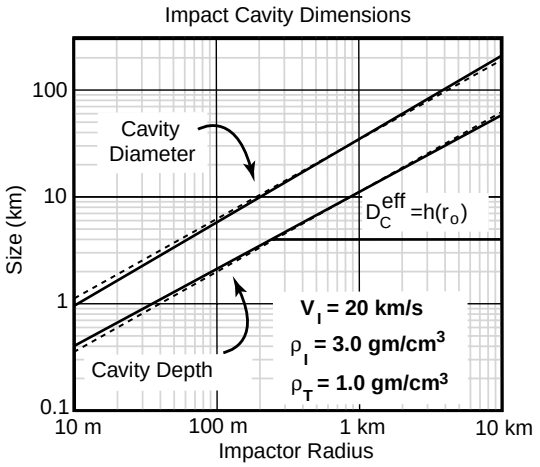

Fig. 2. Plot of initial cavity diameter $d_c(R_I)$ and depth $D_c(R_I)$ versus impactor radius. The solid lines come from Eqs. (7)–(9). The dashed lines come from approximations (10) and (11). For tsunami calculations, we use an effective cavity depth D_c^{eff}. D_c^{eff} equals the actual cavity depth, if $D_c(R_I)$ does not exceed the ocean depth at impact site $\mathbf{r}_0$, otherwise $D_c^{eff} = h(\mathbf{r}_0)$.

site, regardless of the $D_c(R_I)$ predicted from (7)–(9). Otherwise, (2) could predict huge tsunami from impacts into puddles. To accommodate this argument, we set in (6) $D_c = D_c^{eff} = \min[D_c(R_I), h(\mathbf{r}_0)]$. The effective cavity depth D_c^{eff} equals the actual cavity depth if $D_c(R_I)$ does not exceed the ocean depth at impact site $\mathbf{r}_0$. If the actual cavity depth exceeds the ocean depth, then D_c^{eff} reverts to $h(\mathbf{r}_0)$. Note that although effective cavity depth is limited, the diameter $d_c(R_I)$ of the cavity continues to grow indefinitely with impactor radius. Physically, the transition from $D_c^{eff} = D_c(R_I)$ to $D_c^{eff} = h(\mathbf{r}_0)$ coincides with a drop in the efficiency of tsunami production from impactors that "bottom out" in the seafloor. Let $\varepsilon = E_T/E_I$ be the ratio of tsunami energy to impactor kinetic energy. For initial cavities of form (1), Eqs. (9) and (10) of Ward and Asphaug (2000) indicate that the dependence of ε on impactor radius follows the proportion

$$\varepsilon(R_I) \propto [D_c^{eff} R_C(R_I)]^2/R_I^3 \propto [D_c^{eff}]^2/R_I^{3/2}. \quad (12)$$

The second step above comes from (10), the approximate version of (7). Because $D_c(R_I)$ also, is roughly proportional to $R_I^{3/4}$, $\varepsilon(R_I)$ in our model

takes two forms

$$\varepsilon(R_I) \propto [D_c^{\text{eff}}]^2/R_I^{3/2} \propto \text{constant}; \quad D_c(R_I) < h(\mathbf{r}_0), \tag{13a}$$

$$\varepsilon(R_I) \propto [D_c^{\text{eff}}]^2/R_I^{3/2} \propto h^2(\mathbf{r}_0)/R_I^{3/2}; \quad D_c(R_I) > h(\mathbf{r}_0). \tag{13b}$$

For impacts that do not bottom out, (13a) says that the fraction of impactor energy transferred into tsunami is independent of bolide size. For impacts that do bottom out, (13b) says that a smaller and smaller fraction of impactor energy transfers to ocean waves as bolides get larger. Rather, larger impactors spend much of their energy blowing away the seabed.

3. Simulation of the Eltanin Asteroid tsunami

Eqs. (2) and (7)–(9) can simulate tsunami at any distance from impacts of any radius, density and impact velocity. In this note, tsunami from the Eltanin impact take stage. To keep things simple, let us consider direct waves only, and ignore reflections and diffractions. The latter waves are more difficult to compute, and their amplitudes generally far less than the direct ones. In the absence of reflections and diffractions, for a site to experience a tsunami, it must have an unobstructed view (along a ray path) of the impact site. Fig. 3 pictures the direct waves stirred from a 4 km diameter visitor ($\rho_I = 3\,\text{gm/cm}^3$) landing at 20 km/s in the South Pacific Ocean. For this bolide, Eqs. (7)–(9) call for an initial cavity diameter of 60 km and initial cavity depth of 18.4 km.Keeping with our effective depth assumption, D_c^{eff} was reduced to match the 4966 m depth of the ocean at the impact site (57.78°S, 90.79°E). The tsunami mapped in Fig. 3 contain wavelengths as short as 45 km (170 s period). The impact excites shorter waves, but these travel far slower and have smaller amplitude than the main band of waves shown. This calculation also incorporates a variable depth ocean so that shoaling factor (5) causes tsunami to grow on approach to shallow water.

After 1 h (Panel 1, Fig. 3), the impact tsunami has expanded to 750 km. The waves constitute a nearly circular ring because of the relatively uniform ocean depth. The signature of dispersion is clear, with long waves leading the group, and shorter ones lagging. Dispersion plays a heavy role in attenuating impact tsunami. At fixed initial cavity depth, smaller diameter cavities suffer stronger dispersion than larger diameter ones and the tsunami from smaller cavities decay faster with distance. In all cases, peak tsunami amplitude coincides with waves of length roughly equal to the diameter of the initial cavity. Such waves usually do not arrive first. In the situation shown in Panel 1, peak tsunami heights of 280 m locate a few cycles back in the wave packet.

After $2\frac{1}{2}$ h (Panel 2 Fig. 3), the waves have spread to 1750 km and have contacted the shores of South America and Antarctica. The expanding tsunami ring is oblong now, as faster waves move out toward the southwest and slower waves begin to cross the East Pacific Rise toward the northwest. Shoaling amplifications begin to show too. Toward the southwest, where the ocean has the same depth as at the impact site, wave heights peak at 110 m. In the shallower water over the East Pacific Rise, waves build to 130 m. The continental shelves of South America and Antarctica induce far more dramatic shoaling. Waves there hit squarely on, and rise over several cycles to 200–300 m.

After 5 h (Panel 3, Fig. 3), the waves extend to 3500 km. The north-directed component races along parallel to the Chilean coast while the southeast-directed component cuts across the mouth of the Ross Sea. Toward the east, waves have traversed the Drake Passage and look as if they have grounded themselves on the shallows of the Scotia arc. Typical deep-ocean wave amplitudes are 65 m. Shallower areas see heights near 150 m. Impact tsunami of this size may have been sufficient to destabilize regional ice sheets of the period.

After 10 h (Panel 4, Fig. 3), the tsunami reach to 6000 km. Waves 35–40 m tall fast approach Central America, Fiji and Tasmania, and 60 m breakers beach on New Zealand. Waves of 30–40 m slip into the eastern Atlantic, but with their coherence heavily disrupted.

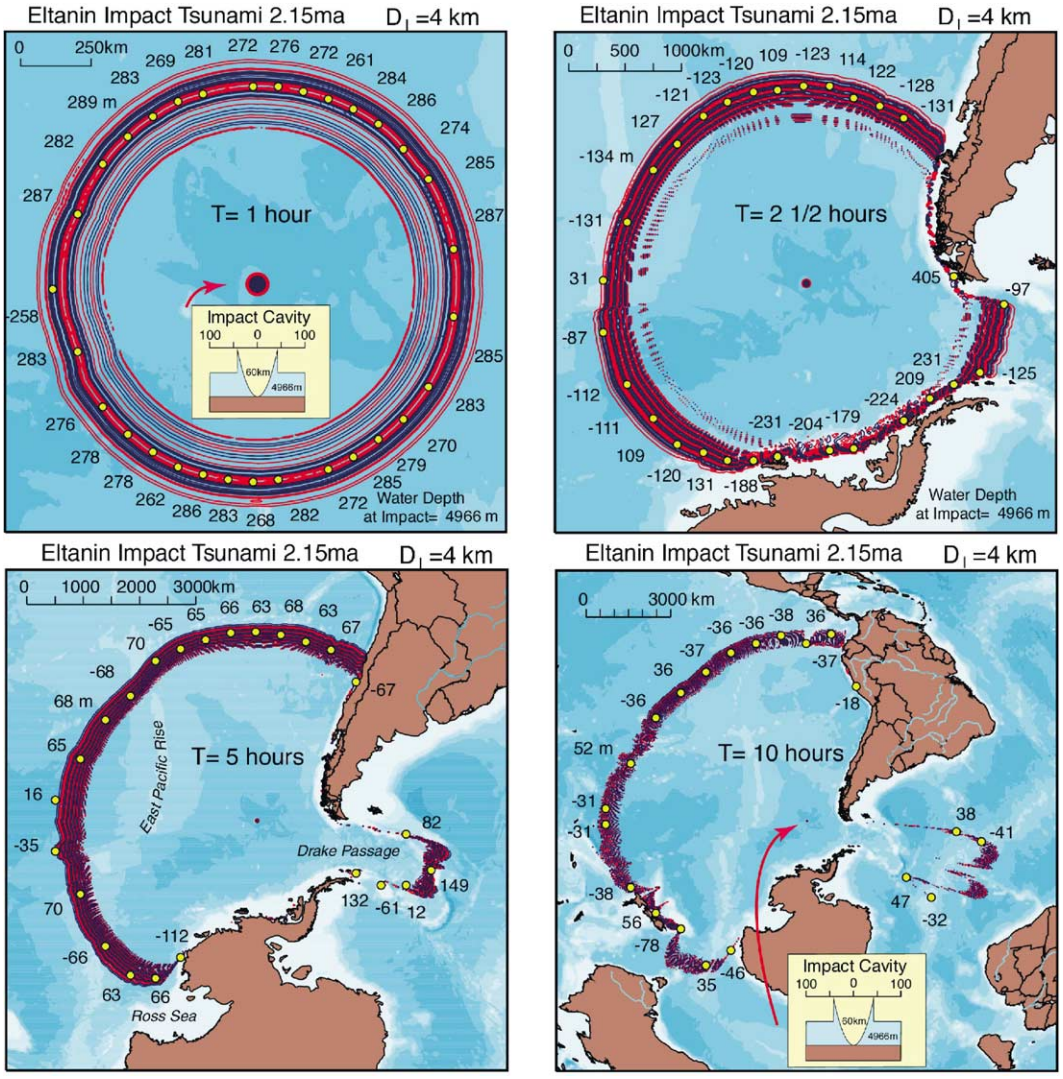

Fig. 3. Simulation of the tsunami from the Eltanin asteroid impact 2.15 Ma. Red and blue color elevated and depressed ocean surfaces respectively. The yellow dots and numbers sample the wave height in meters. The central dot in each panel shows the initial parabolic cavity at true scale. The minimum contours are ± 25 m. Note that no reflected or diffracted waves are included in this figure.

4. Impact tsunami attenuation curves

Scenarios like Fig. 3 wonderfully illustrate impact tsunami, but they are time-consuming to compute. In discussions that reduce to maximum impact tsunami amplitude, it is advantageous to distill the full waveform calculations to an expression that can be run quickly under different conditions—smaller impactor radius for instance. Toward this end, Ward and Asphaug (2000) proposed impact tsunami attenuation curves of the form

$$u_z^{\max}(\mathbf{r},\mathbf{r}_0,R_I) = D_c^{\text{eff}}\sqrt{\frac{\Delta}{\sin\Delta}}\left[1+|\mathbf{r}-\mathbf{r}_0|/R_C\right]^{-\psi},$$

$$\psi = 1/2 + 0.575e^{-0.035R_C/h(\mathbf{r}_0)}. \quad (14)$$

The parts of (14) are understood easily. The first, D_c^{eff}, is the effective cavity depth—the lesser of $D_c(R_I)$ the actual cavity depth computed from

(7)–(9), or (11) or the ocean depth at the impact site. The second, is the spherical correction factor for geometrical spreading (4). The last term is essentially the inverse of the tsunami travel distance raised to a power $\psi \geqslant 1/2$. The two members in ψ account for wave amplitude loses from geometrical spreading on a plane ($|\mathbf{r}-\mathbf{r}_0|^{-1/2}$) and for additional losses due to dispersion. The latter depends on the ratio of cavity radius to ocean depth. For very wide cavities, the added dispersion loss tends toward zero. For very narrow cavities, the added dispersion loss approaches that prompted by geometrical spreading. Ward and Asphaug (2000) derived the two parameters (0.575 and 0.035) from fitting Eq. (14) to peak tsunami heights measured from waveforms (2) at various distances. That fitting employed impactors of 10 to 500 m radius, but judging from the good reproduction of the wave sizes in Fig. 3 (*stars*, Fig. 4), formula (14) seems applicable to bigger impactors too.

Fig. 4 plots attenuation relation (12) for distances between 1 and 10,000 km from impactors of 100 m–10 km diameter. Again, the velocity and density of the impactor were set at 20 km/s and 3 gm/cm^3. (It is a snap to compute other cases.) The Eltanin asteroid is thought to have been between 1 and 4 km diameter (Gersonde et al., 1997). At distances greater than 1000 km, the attenuation curves indicate that a 1 km impactor generates a tsunami about five times smaller than a 4 km impactor. A monster asteroid like Chicxulub (10 km diameter), had it fallen into deep water, would have sent a 100 m tsunami out to 4000 km.

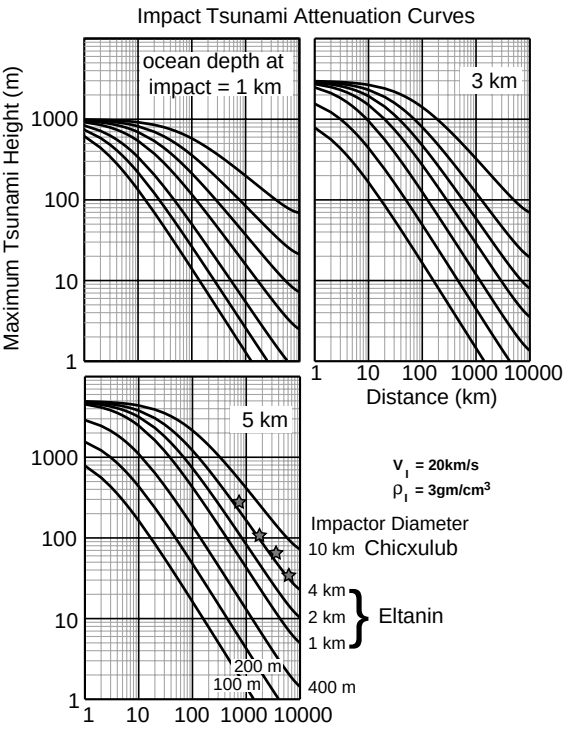

Fig. 4. Peak tsunami height computed from formula (12) versus distance and impactor diameter in oceans of $h(\mathbf{r}_0) = 1$, 3 and 5 km depth. The stars in Panel 3 mark peak tsunami amplitudes read from Fig. 3 at positions where ocean depth $h(\mathbf{r}) \approx h(\mathbf{r}_0)$. These curves do not include shoaling amplification factor (5). Green's law $[h(\mathbf{r}_0)/h(\mathbf{r})]^{1/4}$ provides a quick approximation to this factor.

5. Concluding statement

Asteroid and comet impacts into Earth's oceans are common geologically. Shoemaker et al. (1990) estimated that "on average", a 1-km diameter or larger object strikes the Earth once per 100,000 years. In a given million-year period then, tsunami larger than 100 m should shoal over some regional shoreline several times. Classical theory and simple assumptions about initial cavity shape make the calculation of tsunami from these impacts straightforward. Linear tsunami theory may not hold in every situation, but if nothing else, it fixes a well-documented reference to compare predictions from various non-linear approaches.

Acknowledgements

SNW was supported by Southern California Earthquake Center Award 662703 and NSF Contract EAR-9804970. EIA was supported by the NASA Planetary Geology and Geophysics Program.

References

Ben-Menahem, A., Singh, S.J., 1981. Seismic Waves and Sources. Springer-Verlag, New York.

Dingemans, M.W., 1997. Water Wave Propagation Over Uneven Bottoms, Part-1 Linear Wave Propagation. World Scientific, Singapore.

Gersonde, R., Kyte, F.T., Bleil, U., Diekmann, B., Flores, J.A., Gohl, K., Grahl, G., Hagen, R., Kuhn, G., Sierro, F.J., Völker, D., Abelmann, A., Bostwick, J.A., 1997. Geological record and reconstruction of the late Pliocene impact of the Eltanin asteroid in the southern ocean. Nature 390, 357–363.

Schmidt, R.M., Holsapple K.A., 1982. Estimates of crater size for large-body impacts: Gravitational scaling results. GSA Special Paper 190, GSA, Boulder, pp. 93–101.

Shoemaker, E.M., Wolfe, R.F., Shoemaker, C.S., 1990. Asteroid and comet flux in the neighborhood of Earth. In: Sharpton, V.L.,Ward, P.D. (Eds.), Global Catastrophes in Earth History, GSA Special Paper 247, GSA, Boulder, pp. 155–170.

Ward, S.N., 2001a. Tsunamis. In: Meyers, R. A. (Eds.), The Encyclopedia of Physical Science and Technology. Vol. 17, Academic Press.

Ward, S.N., 2001b. Landslide Tsunami, Journal of Geophysical Research 106 (B6), 11, 201–11, 216.

Ward, S.N., Asphaug, E., 2000. Asteroid impact tsunami: a probabilistic hazard assessment. Icarus 145, 64–78.